Talanta 268 (2024) 125292

Contents lists available at ScienceDirect

Talanta

journal homepage: www.elsevier.com/locate/talanta

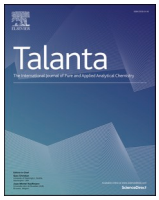

A fully automated Lab-on-a-Disc platform integrated a high-speed triggered siphon valve for PBMCs extraction

Jiahao Zhang [a,b,c], Junyu Ma [a,b], Yang Xu [a,b,e], Yihui Wu [a,b,e,*], Mingshu Miao [d]

[a] State Key Laboratory of Applied Optics, Changchun Institute of Optics, Fine Mechanics and Physics, Chinese Academy of Sciences, Changchun, Jilin, 130033, China
[b] Key Laboratory of Optical System Advanced Manufacturing Technology, Chinese Academy of Sciences, Changchun Institute of Optics, Fine Mechanics and Physics, Changchun, Jilin, 130033, China
[c] University of Chinese Academy of Sciences, Beijing, 100049, China
[d] Department of Clinical Laboratory, The Second Hospital of Jilin University, Changchun, Jilin, 130041, China
[e] GD Changguang Zhongke Bio Co., Ltd., Foshan, Guangdong, 528200, China

ARTICLE INFO

Handling Editor: J. Wang

Keywords:
PBMCs
Lab-on-a-Disk
Percoll
High-speed triggered siphon valve
Clock channel

ABSTRACT

Human Peripheral Blood Mononuclear Cells (PBMCs) are isolated from peripheral blood and identified as any blood cell with a round nucleus that exhibits immune responses and undergoes immunophenotypic changes upon exposure to various pathophysiological stimuli. Obtaining high-recovery and clinical-grade PBMCs without decreasing cell viability and causing stress is crucial for disease diagnosis and successful immunotherapy. However, traditional manual PBMCs extraction methods rely on manual intervention with less recovery rate and reliability. In this study, we introduced a novel and efficient strategy for the fully automated extraction of PBMCs based on a Lab-on-a-Disk (LoaD) platform. The centrifugal chip used percoll as density gradient media (DGM) for separation and extraction on account of the density difference of cells in whole blood, without labeling and any additional extra cellular filtration or cell lysis steps. Above all, we proposed a high-speed triggered siphon valve, which was closed under the speed of cell sedimentation and subsequently opened by increasing speed to complete the extraction of PBMCs. It can avoid the problem that previous siphon valves rely on unstable hydrophilic surface treatment and prime under low/zero speed conditions. With valves and the clock channel integrated on the chip, users can achieve fully automated collection of PBMCs. Compared with the clinical laboratory results, the recovery rate of extracted PBMCs was 80 %. The experimental results prove that the high-speed triggered siphon valve improves the extraction efficiency of PBMCs. The robust chips, which are not only simple to manufacture and assemble but also stable and reliable to use, have great potential in biomedical and clinical applications.

1. Introduction

The isolation and extraction of PBMCs from whole blood for enumeration and analysis are of great significance. PBMCs are not only highly advantageous for the evaluation of certain cancers [1,2], autoimmune diseases [3,4], infectious diseases, and other clinical diseases, but also fundamental to immunotherapy [5,6]. However, isolation and culture of cells used for immunotherapy depend on obtaining PBMCs with high recovery and purity. The extensive clinical requirements of PBMCs inevitably promote the development of non-invasive, automated, and standardized cell isolation techniques. Generally, cell isolation approaches exploit different cell types that differ in physical properties or biochemical specificities, allowing the separation of cells into distinct subpopulations. Traditional techniques rely on red blood cell lysis, fluorescent labeling and staining. From overall consideration of efficiency, purity, and cost, density gradient centrifugation has become one of the most frequently-used separation methods for the extraction of leukocyte subsets [7–11].

DGM utilizes the difference in density between PBMCs, erythrocytes, and granulocytes. Table 1 shows the density and radius of individual cells in human peripheral blood. As shown in Fig. 1, manual procedures in medical laboratories include sequential DGM and blood sample loading, centrifugal separation, plasma removal, and PBMCs layer extraction [12]. However, loading samples and accurately extracting the

* Corresponding author. State Key Laboratory of Applied Optics, Changchun Institute of Optics, Fine Mechanics and Physics, Chinese Academy of Sciences, Changchun, Jilin, 130033, China.
E-mail address: yihuiwu@ciomp.ac.cn (Y. Wu).

https://doi.org/10.1016/j.talanta.2023.125292
Received 27 July 2023; Received in revised form 19 September 2023; Accepted 6 October 2023
Available online 8 October 2023

Table 1
The density range and radius of various blood cells.

Blood cells	Density range(g/ml)	Radius(μm)
Platelets	1.04–1.08 [13]	0.5–2 [14]
Monocytes	1.055–1.066 [15]	6–7.5 [16]
Lymphocytes	1.062–1.077 [15]	3-6 [16]
Basophils	1.075–1.082 [15]	4.5–5 [16]
Neutrophils	1.08–1.09 [15]	6–7.5 [16]
Eosinophils	1.088–1.1 [15]	6–7.5 [16]
Erythrocytes	1.09–1.12 [15]	2.5 [17]

desired cellular components rely on well-trained personnel with their uncertain manual operation. Braking steps in centrifuges inevitably tend to affect the boundary layer in most cases. In addition, experiment personnel require several milliliters of blood to observe and extract leukocyte bands, which may lead to large sample consumption and is not applicable under certain circumstances. Thus, research on obtaining PBMCs layers with fewer blood samples and realizing fully automated extraction with less manual intervention and more cost efficiency is necessary.

Lab-on-a-Disk (so called centrifugal microfluidics) has developed into a mature technology that utilizes a complete set of fluidic unit operations, such as liquid transport [18], metering [19], mixing [20–22], and valving [23–27] to achieve the function of the entire chip [28]. Fluidics in the centrifugal chip is managed by a compact motor which is low-cost and controllable with no pneumatic interface, so it has obvious advantages of integration, automation, miniaturization, and multi-channel. In recent years, the applications of centrifugal microfluidics to extract PBMCs with DGM have sprung up. David J. Kinahan et al. [29] proposed a general description of the centrifugal-pneumatic siphon valve (Centrifugo-Pneumatic Siphon Valving, CPSV) scheme for blood treatment. After the siphon was triggered, a large number of PBMCs seemed to remain in the blood processing room. Compared with hospital laboratory results, extraction efficiency was relatively low at only 34 %; Rokon Uddin [30] similarly used DGM and CPSV to separate the blood sample into plasma and PBMCs while the latter were not extracted from the chip, but directly counted with an automatic optical imaging device. In contrast, the counting efficiency of this scheme can reach about 73 %. As low-pass siphon valves, CPSVs withstand the strong centrifugal field during blood separation and open towards low spin rates [29]. Due to low-speed driving when CPSVs prime, the cell layers will disperse upwards and become disordered under pneumatic function, which restrict applications of CPSVs in density gradient centrifugation. Meisam Madadi et al. [31] proposed an automated model based on DGM using hydrophilic valves on microfluidic discs. However, hydrophilic modification can lead to inherent issues in fabrication, assembly, and long-term stability [32,33], and these strategies may encounter problems with low-pass valves, similarly.

This study aims to realize a siphon scheme independent of hydrophilic modification or low-speed priming, and achieve fully automated high-efficiency extraction of PBMCs. To achieve this goal, the clock channel was presented whose delay effect was verified by simulation, so that DGM and whole blood flowed uniformly from the inlet to the sedimentation chamber. Then, a stable high-speed triggered siphon valve was presented, which suppressed the tendency of cells to disperse upwards by means of large centrifugal force during the siphoning process and thus improved the PBMCs extraction efficiency. The LoaD platform maintained milder centrifugation conditions (150×*g* for 8 min) compared with traditional manual methods (800×*g* for 20 min), and recovery of the isolated PBMCs is higher and reproducibility is better. Furthermore, this chip holds potential for the convenient addition of similar series-wound extraction chambers to separate more components with percoll's advantages of separating multilayer cells. Hence, this platform can extract and provide valuable resources for PBMCs or other target cells, which has strategic significance for further applications in the future.

2. Materials and methods

2.1. Samples and reagents

Phosphate buffered saline (1 × PBS, pH7.4), 5 M NaCl (1.190 g/cm^3), Endotoxin-free ultra pure water, percoll (1.13 g/ml±0.005 g/ml, pH8.5–9.5) were purchased from Sigma-Aldrich (Sigma-Aldrich, St. Louis, MO, USA) for efficient isolation of PBMCs. EDTA (Thermo Fisher Scientific, USA) processed blood samples were drawn from healthy subjects from the Second Hospital of Jilin University (Changchun, China). Prior to each experiment, the blood was slowly oscillated to homogenize the cells, and then 15 μl was diluted 1:1 with PBS solution. Pressure Sensitive Adhesive (PSA) was purchased from Sekisui Chemical (Sekisui Chemical Co., Ltd., Osaka, Japan).

2.2. Preparation of DGM

The density gradient media of percoll in demand was prepared with a universal technique which was exhaustively described by the product sheet from Sigma. Endotoxin-free ultra pure water was used to dilute 5 M NaCl and obtained 1.5 M NaCl and 0.15 M NaCl, respectively. The

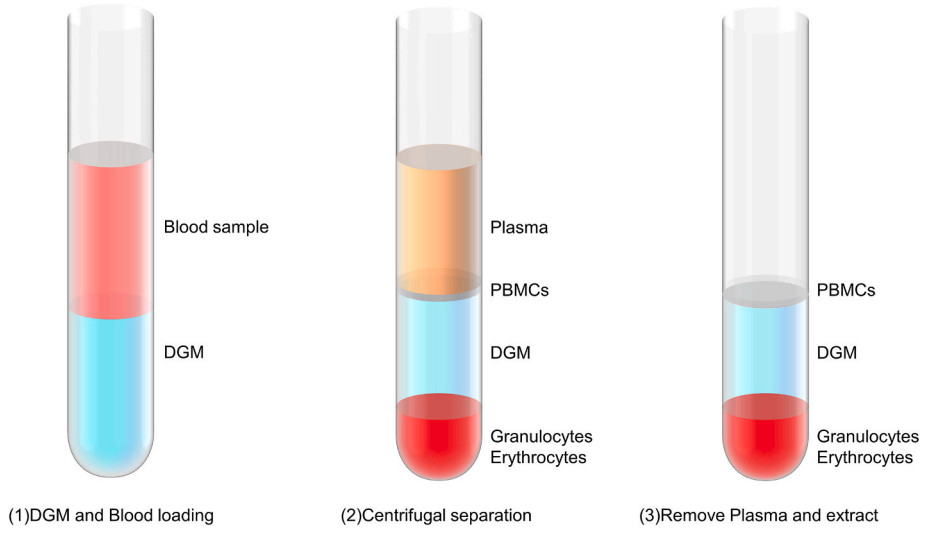

Fig. 1. Manual density gradient centrifugation methods.

100 % stock isotonic percoll (SIP) (1.123 g/ml) was prepared by mixing 1:9 vol ratio of 1.5 M NaCl to stock percoll (1.13 g/ml). The gradient media with the final density of 1.077 g/ml was prepared by diluting 60 % of SIP using 0.15 M NaCl. To prevent bacterial reproduction, the percoll gradient media was kept at 4 °C and recovered to room temperature before use and mixed well.

2.3. Chip design

The Chip consisted of five array units. Fig. 2a showed that one unit was composed of DGM and blood loading chamber, a smaller DGM storage chamber, extraction chamber, waste chamber, and other microchannels. DGM loading chamber was directly connected with the sedimentation chamber which was used for blood processing and the clock channel connected the blood loading chamber and the sedimentation chamber. The sedimentation chamber vent was also designed to better circulate the air inside the chamber to facilitate the layering of blood cells. The smaller DGM storage chamber was linked by a long microchannel with the sedimentation chamber and its priming speed under blood processing speed was restrained by a capillary valve. The principle of the capillary valve involves using capillary pressure to restrain the progression of the liquid. By controlling the rotation speed of the chip to establish a balanced relationship between the appropriate centrifugal force and capillary pressure, fluid movement can be regulated. The rotational speed at which centrifugal force can overcome the capillary pressure is referred to as the burst frequency. The formula of the pressure caused by centrifugal force is as follows [34]:

$$P_\omega = \rho\omega^2 \bar{r} \triangle r \tag{1}$$

In Eq. (1), ρ is the density of the liquid, ω (rad/s) is the rotation speed of the chip, $\bar{r}$ is the average radial distance of the liquid plug; Δr is the radial extent of the fluid.

The capillary pressure at the junction is defined [35,36] by the following Eq. (2):

$$P_c = \gamma\left[\frac{2}{h}\left(\frac{\cos^2\theta_{PMMA} - 1}{\cos\theta_{PMMA}}\right) - \frac{1}{w}\right] \tag{2}$$

where γ is the corresponding surface tension, w and h are the channel width and depth, respectively. θ_{PMMA} is contact angle of the solution on PMMA (about 68°). P_c is found to be negative, which stops the liquid flow at the junction.

The liquid will be moved through the valve when the centrifugal force surpasses the capillary force at a specific rotational speed known as the burst frequency. The theoretical burst frequency can be expressed by Eq. (3) as follows [36]:

$$f = \frac{30}{\pi}\sqrt{-\frac{\gamma\left[2/h\left(\frac{\cos^2\theta_{PMMA}-1}{\cos\theta_{PMMA}}\right) - 1/w\right]}{\rho\bar{r}\Delta r}} \tag{3}$$

Obviously, by controlling w, h, $\bar{r}$ and Δr, the desired burst frequency can be achieved. The specific dimensions of the capillary valve are illustrated in Fig. S1, and it is determined through calculations that the theoretical burst frequency is about 2127 RPM.

2.4. Chip fabrication

In the experiments, chips were manufactured using the standard

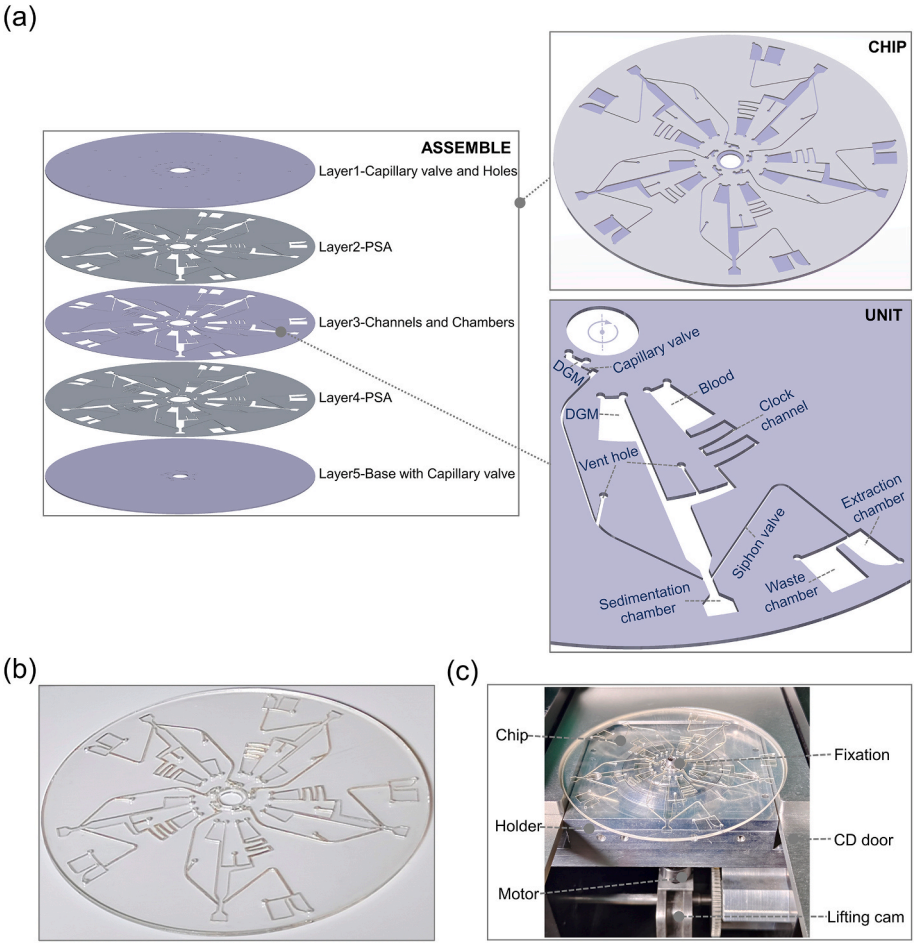

Fig. 2. (a) Assembly and structure of the chip. (b) A photograph of the chip. (c) A centrifugal platform for experiments.

commercial computer-aided design software (AutoCAD 2007, Autodesk, USA). As shown in Fig. 2a, a multi-layer polymer substrate chip with 102 mm diameter was fabricated in the following order: a top layer of polymethyl methacrylate (PMMA) with vent holes was used as the cover layer and the bottom layer with a motor mounting hole was used to encapsulate the chip. The middle layer contained the main structure with microchannels and microchambers, which was pasted with double-layer PSA and connected the top layer and bottom layer, respectively. PMMA thickness was 1.5 mm and the capillary valve was expanded across all three layers. Microchannels and chambers structure on the middle layer were cut using CO_2 Laser engraving system (TROTEC, Speedy 100R, Australia), and both the top and bottom layers were cut to obtain each through hole after creating capillary valve structures by engraving. The bonding of the chip was completed with PSA. Before sealing, the chip was rinsed with deionized water and finally dried under a stream of nitrogen gas. This process was repeated up to three times. Then, the PMMA and PSA layers were pasted sequentially in a bottom-up assembly method. Finally, the suction hole on the extraction chamber were sealed with adhesive tape before use. Fig. 2b showed an example of a prepared microfluidics chip. The chips were tested on a centrifugal platform that had the function of automated chip loading (Fig. 2c).

2.5. Numerical simulation method

Conventional density gradient centrifugation methods require the sequential loading of DGM and the diluted whole blood sample. Furthermore, laying the sample gently and steadily on DGM is indispensable to create a clear interface before centrifugation for blood processing. For this purpose, it is necessary to slow down the flow rate of the whole blood sample before it enters the sedimentation chamber. The fluid flow velocity is inversely proportional to the hydrodynamic resistance which is related to the characteristic dimensions and the channel length. Increasing the length of microchannels or reducing the width and depth of microchannels can decrease the fluid flow velocity. Therefore, according to this principle, the microchannel structure characteristics were controlled to regulate the time required for liquid loading into the sedimentation chamber. To determine the appropriate dimensions of the clock channel and validate the feasibility of flow retardation, a two-phase flow level set method was used to simulate the flow process of the storage chamber and sample chamber.

This study used a laminar incompressible flow model with no-slip boundary conditions to determine the flow field. Based on the Navier–Stokes equation for incompressible fluids, Eq. (4) and Eq. (5) used to simulate the mass and momentum transfer of fluid [37] are:

$$\rho\frac{\partial \vec{u}}{\partial t}+\rho(\vec{u}\cdot\nabla)\vec{u}=\nabla\cdot\left[-p\vec{I}+\mu(\nabla\vec{u}+(\nabla\vec{u})^{T})\right]+\vec{f} \tag{4}$$

$$\nabla\cdot\vec{u}=0 \tag{5}$$

where ρ is the fluid density, $\vec{u}$ is the fluidic velocity vector, μ is the dynamic viscosity of the fluid, p is the pressure, $\vec{I}$ is the unitary tensor, and $\vec{f}$ which is the sum of $\vec{F}_{Cen}$ and $\vec{F}_{Cor}$ in the centrifugal chip, is the volume force acting on the fluid.

The level set method can describe the coupling interface between gas and liquid which are distinguished with Φ. The level set function can be viewed as the volume fraction of liquid. The propagation of the interface between the two-phase flow and initialization of the level set function are controlled by Eq. (6):

$$\frac{\partial\Phi}{\partial t}+\vec{u}\cdot\nabla\Phi=\gamma\nabla\cdot\left(\varepsilon\nabla\Phi-\Phi(1-\Phi)\frac{\nabla\Phi}{|\nabla\Phi|}\right) \tag{6}$$

where ε is the parameter that determines the thickness of the interface, and can usually be specified as $\varepsilon = h_c/2$, where h_c represents the characteristic size of the interface grid, γ represents the number of reinitializations, and is typically set as the maximum velocity value in the model.

Under continuum mechanics and Eulerian description conditions, a dynamic model of air-liquid interaction based on the level set method was established. Considering the incompressibility of the fluid in the chip, the Newtonian fluid model was used to simulate the mass and momentum transfer of the chip fluid with the Navier-Stokes equation, while considering the influence of the surface tension of the air and liquid interfaces, The Navier-Stokes equation and the continuity equation are given as Eq. (7) and Eq. (8):

$$\rho\frac{\partial \vec{u}}{\partial t}+\rho(\vec{u}\cdot\nabla)\vec{u}=\nabla\cdot\left[-p\vec{I}+\mu(\nabla\vec{u}+(\nabla\vec{u})^{T})\right]+\vec{f}_{st}+\vec{f} \tag{7}$$

$$\nabla\cdot\vec{u}=0 \tag{8}$$

where $\vec{I}$ is the unified tensor, $\vec{f}$ is the volume force acting on the fluid in the centrifugal chip, and $\vec{f}_{st}$ is the surface tension at the air-liquid interface. In the level set interface, the surface tension is

$$\vec{f}_{st}=\sigma\delta\kappa\vec{n} \tag{9}$$

In Eq. (9), σ is the surface tension coefficient, δ is the Dirac function, $\kappa=-\nabla\cdot\vec{n}$ is the curvature, and $\vec{n}$ is the interface normal.

For the fluid inlets, outlets and air vents of the fluid domain, we adopted open boundary conditions, whereas no-slip boundary conditions were applied to all other boundaries.

In the experiment, the area of the DGM chamber and blood chamber was set to 75 mm^2, the depth was 0.2 mm, the width of the channel directly connected to the DGM chamber was 0.8 mm, and the width and length of the clock channel were respectively 0.4 mm and 30 mm. In the simulation, colors represent the volume fraction of air. At the initial state (t = 0 s), the chambers were full of liquid, with an air volume fraction of 0 which appeared entirely blue. As the liquid flowed out, the color gradually turned red, representing the air replacing the original liquid inside the chamber. (Fig. 3). The results showed that the descent rate of the liquid level in DGM chamber was obviously faster than that in the blood chamber. When the liquid in the DGM chamber was exhausted, the liquid in the blood chamber filled up the clock channel and prepared to enter the sedimentation chamber. This theoretically confirmed the adequate functionality of the clock channel in achieving sequential control of liquid flow and validated the feasibility of the above design approach.

3. Results and discussion

3.1. Experimental procedures on chip

First, a fixed volume of percoll and the diluted blood sample were injected into DGM chamber and blood chamber using a pipette, respectively, as shown in Fig. 4 I, i. Then, the centrifugal platform was controlled to spin at a fixed acceleration, thus the centrifugal force generated by the rotation drove the flow of DGM and blood sample. Due to the presence of a long curving channel below the blood chamber, the flow velocity of the sample was reduced, while the wide straight channel below DGM chamber facilitated the rapid loading of percoll into the sedimentation chamber. After percoll was fully loaded, the blood sample had just filled the clock channel and began to flow smoothly into the sedimentation chamber along the wall (Fig. 4 II, ii). With the stable spin rate, cells of different densities started to sediment and layer under the influence of DGM. The total liquid volume height in the sedimentation chamber should be less than the radial height of the siphon valve crest-point to prevent untimely priming during blood processing (Fig. 4 III, iii). After cells layering, DGM in the capillary valve near the rotation center surpassed its burst frequency by further increasing the spin rate

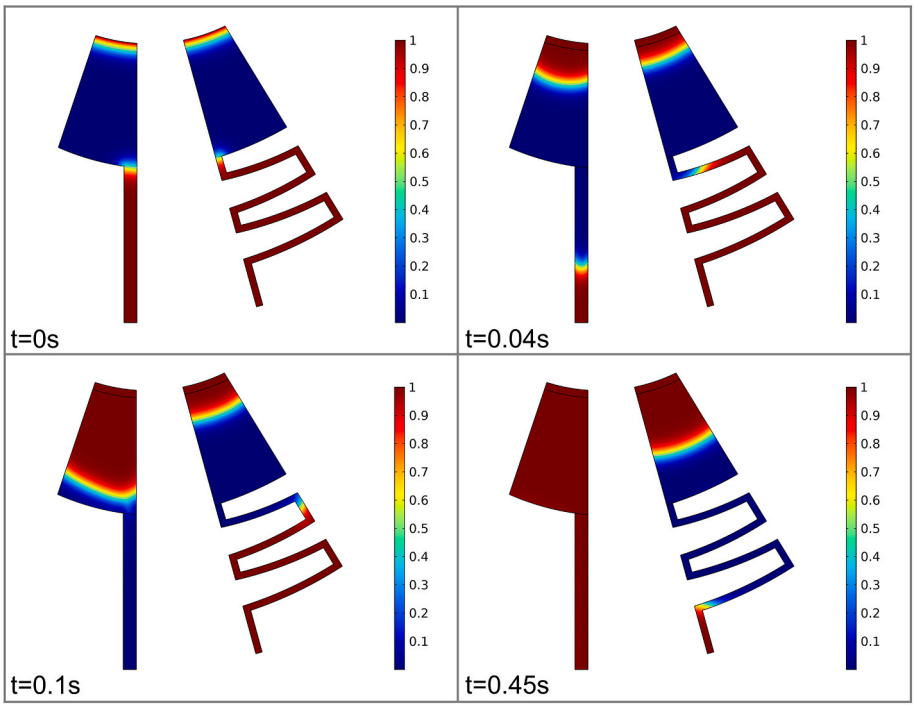

Fig. 3. Simulation of fluidics in the clock channel. The color change represents the variation in air volume fraction.

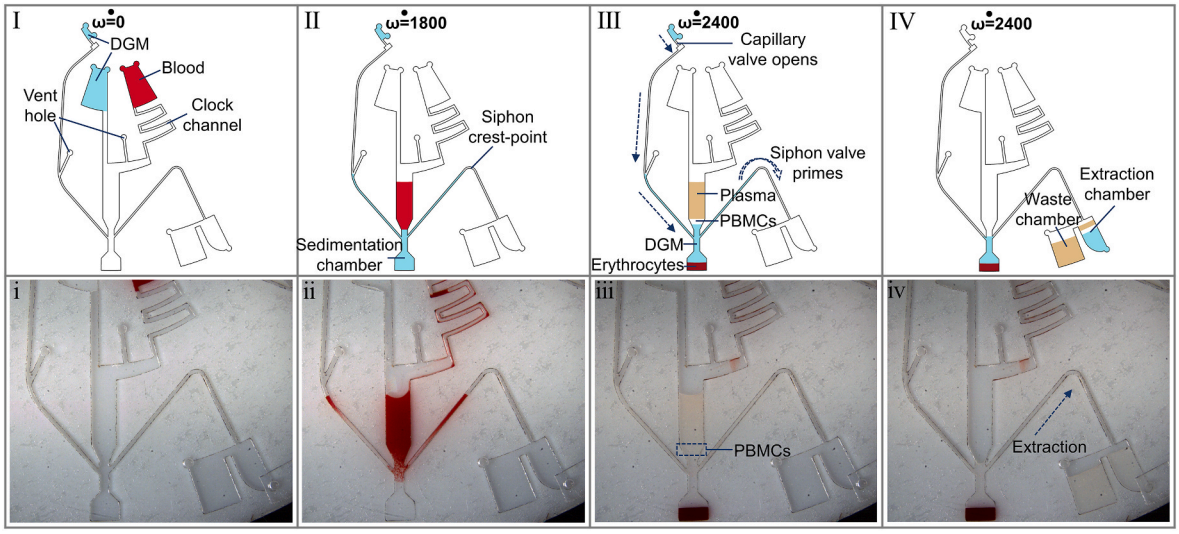

Fig. 4. Two groups of images (I-IV) and (i-iv) show the process performed on a microfluidic chip. (I, i) The position of DGM and the diluted blood sample prior to the initiation of rotation. (II, ii) Through the impact of the clock channel, DGM was fully loaded into the sedimentation chamber while the whole blood had not entered yet. With continuity of rotation, the blood gently and steadily flowed into the sedimentation chamber, layering on top of percoll. Subsequently, the liquid level reached the crest-point of the siphon valve, resulting in a relatively stable state. (III, iii) Blood processing finished, forming a layer of red blood cells and granulocytes, a layer of DGM, a layer of PBMCs, and a layer of plasma in the sedimentation chamber. Additionally, platelets distribute within PBMCs and plasma layers. The arrows indicated the direction of flow in the valves. (IV, iv) The spin rate was increased, and the capillary valve next to the rotation center opened. Then additional 3 μl percoll that generated pinched flow caused the liquid level in the sedimentation chamber to rise and the siphon valve started to prime later. The high-speed rotation continued to transfer DGM, PBMCs layer, and plasma into the extraction chamber, while excess plasma was transferred to the waste chamber.

and entered the sedimentation chamber along the channel. With the liquid level in the sedimentation chamber higher than the crest-point, the siphon valve primed and liquid above the siphon valve began to flow into the extraction chamber. Upon the extraction chamber was full, excess plasma overflowed into the waste chamber (Fig. 4 IV, iv). Finally, PBMCs were collected from the extraction chamber for counting and analysis. To better visualize the fluid motion process, the substrate of this chip was made of opaque PMMA.

3.2. Optimization of spin protocol

In this work, one critical challenge was obtaining an optimized spin protocol for the chip because the forces in the centrifugal field were crucial factors for PBMCs extraction. Before the chip started to rotate, percoll and the sample were injected into the DGM chamber and the blood sample chamber, respectively. After loading on the chip, a step-wise centrifugal movement was initiated to mirror the typical

procedure of a tube test. The slight loading of DGM on the blood is necessary to improve the clarity and stability of the layering. In traditional density gradient centrifugation methods using centrifuge tubes, the speed of the acceleration and deceleration processes must be kept as low as possible to maintain stability of the cell layer. Hence, these methods may slow down the starting or braking process and increase the total handling time. Nevertheless, due to the structural scale reduction of the microfluidics chip, the inertial force decreased and the surface tension relatively increased. Cells were less affected by the Euler force, and not insufficient to overcome the surface tension, resulting in transparent layering. The acceleration speed of the chip was set at a low level of 30 RPM/s. The slower acceleration had no apparent adverse effect on the results but extended the operation time required for the entire procedure. In capillary valve tests, we found that it kept closed under 2000 RPM and opened above 2400 RPM (Table S1). To ensure the stable priming of the capillary valve and reduce cellular stress, we had determined the blood processing speed to be 1800 RPM, while activating frequency of the capillary valve was set at 2400 RPM. The sedimentation process was performed by sustaining the spin rate of 1800 RPM for 8 min. Increasing the sedimentation time or rotation speed did not enhance the efficiency of PBMCs extraction, whereas it may decrease cell viability to a certain extent. The gradual and controlled reduction of spin rate was of paramount importance in preserving the stability of the DGM-PBMCs interface. Once layering was accomplished, the rotation speed was similarly increased at 30 RPM/s to reach 2400 RPM. At this point, the increased centrifugal force acting on the additional 3 μl percoll caused it to break through the capillary valve and enter the sedimentation chamber. Subsequently, the liquid level rose, triggering the siphon valve. By maintaining the speed at 2400 RPM, the PBMCs layer started to leave the sedimentation chamber and entered the extraction chamber, while excess liquid was transferred to the waste chamber. After the experimental process was accomplished, the chip stopped rotating. The optimized spin protocol on the chip is shown in Fig. 5.

3.3. Cell extraction analysis

After completing the separation of the target cells band, the chip was placed under a high-speed camera and observed using a 10X objective lens (Olympus, Japan) to assess the sorting effectiveness accurately. During the observation, it was found that the extraction chamber contained almost entire PBMCs and some platelets, with no contamination with erythrocytes (Fig. 6a). The PBMCs were uniformly dispersed and in good condition, demonstrating that the spin protocol determined in the above experiments had minimal impact on cell damage. Only a few platelets and PBMCs were present in the waste chamber (Fig. 6b), indicating that the target layer in the sedimentation chamber did not experience significant disruption during the siphoning process. The target layer entered the extraction chamber stably, without causing loss of PBMCs.

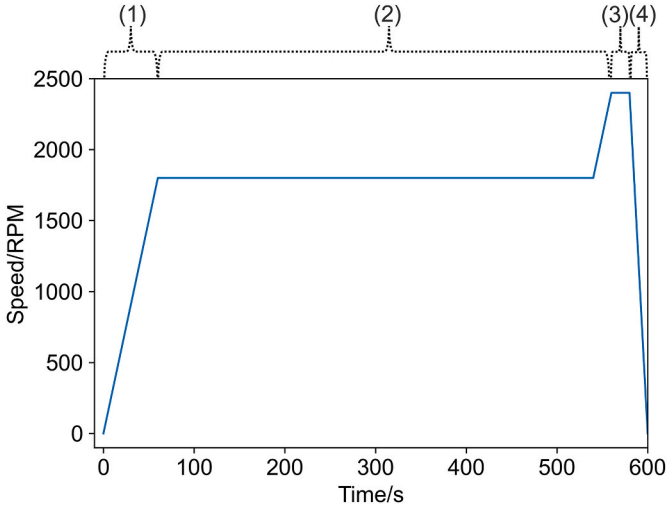

Fig. 5. Optimized step-wise spin protocol for PBMCs extraction. (1) Accelerated at 30 RPM/s to 1800 RPM and introduced DGM and the blood sample into the sedimentation chamber; (2) Spun at 1800 RPM for 480 s to process blood thoroughly; (3) Accelerated at 30 RPM/s again to 2400 RPM, the capillary valve burst and then the siphon valve primed; (4) Maintained the speed of 2400 RPM and transported PBMCs into the extraction chamber.

In order to prove the effectiveness of PBMCs extraction, cells extracted from 15 μl whole blood were recovered from the chip, resuspended in buffer homogenously and then enumerated using a hemocytometer (Millicell® Disposable Hemocytometer, Sigma-Aldrich, USA). Fig. 7a shows the counting result using a color camera (DP74, Olympus, Japan). Fig. 7b displays the PBMCs count/μl from samples collected from healthy subjects, and compares the PBMCs extraction efficiency using the proposed fully automated centrifugal chip with the standard cell counting method in medical laboratories. The result indicates that with the full automated strategy and the modified siphon valve, the extraction efficiency of PBMCs increases to approximately 80 %.

In traditional hydrophilic siphon valves or CPSV strategies, the chips rely on capillary force or pneumatic force at low rotation frequency to drive the liquid across the crest-point. These methods suffer from inherent surface modification issues and result in the upward dispersion of cells under low-speed conditions, leading to the loss of some PBMCs. In contrast, the high-speed triggered siphon valve proposed in this study primed after the additional DGM broke through the capillary valve, entered the sedimentation chamber, and then slightly raised the liquid level. Due to the large centrifugal force during high-speed rotation, the cell layers did not exhibit upward dispersion, and no remaining PBMCs band was observed after siphoning. It indicated that DGM effectively carried PBMCs into the extraction chamber, resulting in an 80 % extraction efficiency. It is inevitable that manual recovery of PBMCs from the extraction chamber causes some loss, which is one reason for the lower extraction efficiency compared to the medical laboratory results. Additionally, there are limitations in using the DGM method for PBMCs extraction, as the DGM cannot separate 100 % of PBMCs [16]. A portion of the remaining PBMCs may also be lost in the sedimentation chamber and valve during the separation process due to surface adsorption of cells and protein. One potential solution is passivating the PMMA surface with the blocker solution or adopting more precise and cleaner manufacturing methods. Because of the low diffusion constant of percoll, the formed gradient is highly stable and can be used for the separation of several cell layers. Further, this chip holds potential for the convenient addition of similar series-wound extraction chambers to separate more components such as monocytes, lymphocytes, and granulocytes. With the integration of five array units, one chip can simultaneously process multiple samples. To ensure the purity of the extracted cells, each unit of the chip is designed for single use.

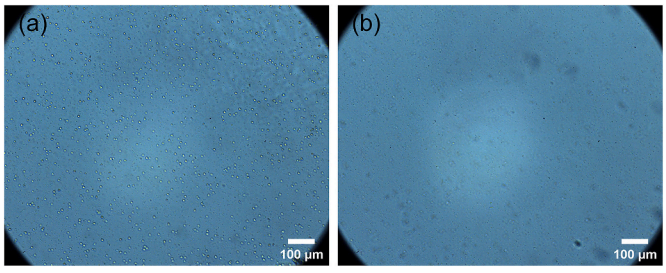

Fig. 6. Image of cells on the chip. (a) The extraction chamber predominantly contained PBMCs, which were uniformly dispersed with sound status. (b) The Waste chamber mainly contained plasma and platelets. All the scale bars were 100 μm.

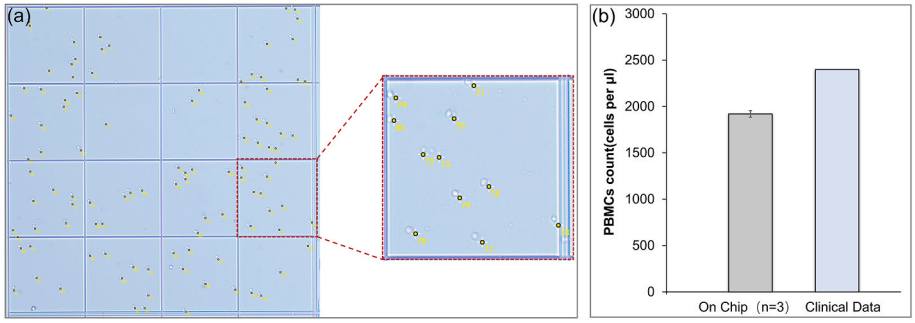

Fig. 7. (a) Extracted PBMC counts. (b) Comparison of results on chip and medical data.

4. Conclusion

In this study, a density gradient centrifugation method based on LoaD was proposed to separate and extract PBMCs. Despite the extensive utilization of cell separation techniques using DGM over the past decades, there has been a notable absence of endeavors focused on customizing these methodologies for seamless and automated integration into the LoaD platform. Compared to traditional manual methods, our results demonstrate a novel system that can automatically isolate intact PBMCs from whole blood with high yield, low pressure, and less than half the time required by manual methods (150×*g* for 8 min vs 800×*g* for 20 min). The integrated clock channel and high-speed triggered siphon valve in this chip fulfill the requirements for an automated system to isolate PBMCs from whole blood. Furthermore, the chip eliminates the reliance on surface treatment in traditional hydrophilic siphon valves and overcomes the issue of target cell loss during transfer on account of the low-pass and unstable factors in CPSV strategies. It enables the precise and efficient separation of the ultra-thin target cell layer from the plasma and DGM layer. With only a dozen microliters of whole blood required, the proposed LoaD platform can be widely used for biological analysis and clinical therapy.

Author contributions

Jiahao Zhang: Methodology, Writing - Original Draft, Visualization, Validation. Junyu Ma: Methodology, Investigation. Yang Xu: Resources. Yihui Wu: Conceptualization, Funding acquisition, Writing - Review & Editing. Minshu Miao: Resources.

Declaration of competing interest

The authors declare that they have no known competing financial interests or personal relationships that could have appeared to influence the work reported in this paper.

Data availability

Data will be made available on request.

Acknowledgements

This work was supported by the National Natural Science Foundation of China (Grant/Award Number: U21A20395) and Strategic Priority Research Program of Chinese Academy of Sciences (Grant/Award Number: XDA22020406).

Appendix A. Supplementary data

Supplementary data to this article can be found online at https://doi.org/10.1016/j.talanta.2023.125292.

References

[1] X. Cheng, A. Gupta, C. Chen, et al., Enhancing the performance of a point-of-care CD4+ T-cell counting microchip through monocyte depletion for HIV/AIDS diagnostics, Lab Chip 9 (10) (2009) 1357–1364, https://doi.org/10.1039/B818813K.
[2] M. Patysheva, I. Larionova, M. Stakheyeva, et al., Effect of early-stage human breast Carcinoma on monocyte programming, Front. Oncol. 11 (2022), 800235, https://doi.org/10.3389/fonc.2021.800235.
[3] A. Picchianti Diamanti, B. Laganà, M.C. Cox, et al., TCD4pos lymphocytosis in rheumatoid and psoriatic arthritis patients following TNFα blocking agents, J. Transl. Med. 15 (1) (2017) 1–6, https://doi.org/10.1186/s12967-017-1135-6.
[4] J. Du, S. Chen, J. Shi, et al., The association between the lymphocyte-monocyte ratio and disease activity in rheumatoid arthritis, Clin. Rheumatol. 36 (2017) 2689–2695, https://doi.org/10.1007/s10067-017-3815-2.
[5] Z. Wang, S. Ahmed, M. Labib, et al., Isolation of tumour-reactive lymphocytes from peripheral blood via microfluidic immunomagnetic cell sorting, Nat. Biomed. Eng. (2023) 1–16, https://doi.org/10.1038/s41551-023-01023-3.
[6] K.K. Dijkstra, C.M. Cattaneo, F. Weeber, et al., Generation of tumor-reactive T cells by co-culture of peripheral blood lymphocytes and tumor organoids, Cell 174 (6) (2018) 1586–1598, https://doi.org/10.1016/j.cell.2018.07.009.
[7] Y. Ukita, T. Oguro, Y. Takamura, Density-gradient-assisted centrifugal microfluidics: an approach to continuous-mode particle separation, Biomed. Microdevices 19 (2017) 1–9, https://doi.org/10.1007/s10544-017-0158-3.
[8] J.M. Park, M.S. Kim, H.S. Moon, et al., Fully automated circulating tumor cell isolation platform with large-volume capacity based on lab-on-a-disc, Anal. Chem. 86 (8) (2014) 3735–3742, https://doi.org/10.1021/ac403456t.
[9] J.M. Park, J.Y. Lee, J.G. Lee, et al., Highly efficient assay of circulating tumor cells by selective sedimentation with a density gradient medium and microfiltration from whole blood, Anal. Chem. 84 (17) (2012) 7400–7407, https://doi.org/10.1021/ac3011704.
[10] Y. Sun, P. Sethu, Low-stress microfluidic density-gradient centrifugation for blood cell sorting, Biomed. Microdevices 20 (2018) 1–10, https://doi.org/10.1007/s10544-018-0323-3.
[11] Y. Sun, P. Sethu, Microfluidic adaptation of density-gradient centrifugation for isolation of particles and cells, Bioengineering 4 (3) (2017) 67, https://doi.org/10.3390/bioengineering4030067.
[12] C. Cui, K.Q. Schoenfelt, K.M. Becker, et al., Isolation of polymorphonuclear neutrophils and monocytes from a single sample of human peripheral blood, STAR protocols 2 (4) (2021), 100845, https://doi.org/10.1016/j.xpro.2021.100845.
[13] M. Milovanovic, K. Lotfi, T. Lindahl, et al., Platelet density distribution in essential thrombocythemia, Pathophysiol. Haemostasis Thrombosis 37 (1) (2010) 35–42, https://doi.org/10.1159/000314964.
[14] C.J. Kim, D.Y. Ki, J. Park, et al., Fully automated platelet isolation on a centrifugal microfluidic device for molecular diagnostics, Lab Chip 20 (5) (2020) 949–957, https://doi.org/10.1039/C9LC01140D.
[15] Z.T.F. Yu, J.G. Joseph, S.X. Liu, et al., Centrifugal microfluidics for sorting immune cells from whole blood[J], Sensor. Actuator. B Chem. 245 (2017) 1050–1061, https://doi.org/10.1016/j.snb.2017.01.113.
[16] S.T. Moen, C.L. Hatcher, A.K. Singh, A centrifugal microfluidic platform that separates whole blood samples into multiple removable fractions due to several discrete but continuous density gradient sections, PLoS One 11 (4) (2016), e0153137, https://doi.org/10.1371/journal.pone.0153137.
[17] E.S. Ofjord, G. Clausen, Intrarenal flow of microspheres and red blood cells: skimming in slit and tube models, Am. J. Physiol. 245 (3) (1983) H429–H436, https://doi.org/10.1152/ajpheart.1983.245.3.H429.
[18] M.M. Aeinehvand, F. Ibrahim, W. Al-Faqheri, et al., Latex micro-balloon pumping in centrifugal microfluidic platforms, Lab Chip 14 (5) (2014), https://doi.org/10.1039/c3lc51116b.
[19] J.N. Klatt, M. Depke, N. Goswami, et al., Tryptic digestion of human serum for proteomic mass spectrometry automated by centrifugal microfluidics, Lab Chip 20 (16) (2020) 2937–2946, https://doi.org/10.1039/D0LC00530D.
[20] J. Lee, S. Lee, M. Lee, et al., Enhancing mixing performance in a rotating disk mixing chamber: a quantitative investigation of the effect of euler and Coriolis forces, Micromachines 13 (8) (2022), https://doi.org/10.3390/mi13081218.

[21] E.S. Shanko, L. Ceelen, Y. Wang, et al., Enhanced microfluidic sample homogeneity and improved antibody-based assay kinetics due to magnetic mixing, ACS Sens. 6 (7) (2021) 2553–2562, https://doi.org/10.1021/acssensors.1c00050.
[22] S. Wang, W. Qi, S. Wu, et al., An automatic centrifugal system for rapid detection of bacteria based on immunomagnetic separation and recombinase aided amplification, Lab Chip 22 (19) (2022) 3780–3789, https://doi.org/10.1039/D2LC00650B.
[23] F. Dal Dosso, L. Tripodi, D. Spasic, et al., Innovative hydrophobic valve allows Complex liquid manipulations in a self-powered channel-based microfluidic device, ACS Sens. 4 (3) (2019) 694–703, https://doi.org/10.1021/acssensors.8b01555.
[24] B.D. Henderson, D.J. Kinahan, J. Rio, et al., Siphon-controlled automation on a lab-on-a-disc using event-triggered dissolvable film valves, Biosensors 11 (3) (2021) 73, https://doi.org/10.3390/bios11030073.
[25] N. Li, M. Shen, Y. Zhu, et al., Euler force-assisted sequential liquid release on the centrifugal microfluidic platform, Sensor. Actuator. B Chem. 359 (2022), https://doi.org/10.1016/j.snb.2022.131642.
[26] R. Mishra, J. Zapatero-Rodriguez, S. Sharma, et al., Automation of multi-analyte prostate cancer biomarker immunoassay panel from whole blood by minimum-instrumentation rotational flow control, Sensor. Actuator. B Chem. 263 (2018) 668–675, https://doi.org/10.1016/j.snb.2018.02.015.
[27] E.M. Arjmand, M. Saadatmand, M.R. Bakhtiari, et al., Design and fabrication of a centrifugal microfluidic disc including septum valve for measuring hemoglobin A1c in human whole blood using immunoturbidimetry method, Talanta 190 (2018) 134–139, https://doi.org/10.1016/j.talanta.2018.07.081.
[28] O. Strohmeier, M. Keller, F. Schwemmer, et al., Centrifugal microfluidic platforms: advanced unit operations and applications, Chem. Soc. Rev. 44 (17) (2015) 6187–6229, https://doi.org/10.1039/C4CS00371C.
[29] D.J. Kinahan, S.M. Kearney, N.A. Kilcawley, et al., Density-gradient mediated band extraction of leukocytes from whole blood using centrifugo-pneumatic siphon valving on centrifugal microfluidic discs, PLoS One 11 (5) (2016), e0155545, https://doi.org/10.1371/journal.pone.0155545.
[30] R. Uddin, M. Donolato, E.T. Hwu, M.F. Hansen, A. Boisen, Combined detection of C-reactive protein and PBMC quantification from whole blood in an integrated lab-on-a-disc microfluidic platform, Sensor. Actuator. B Chem. 272 (2018) 634–642, https://doi.org/10.1016/j.snb.2018.07.015.
[31] M. Madadi, M. Fathipour, J.B. Ghasemi, Separation of human granulocytes and mononuclear cells from whole blood using percoll on a centrifugal microfluidic disc, Microchem. J. 167 (2021), 106316, https://doi.org/10.1016/j.microc.2021.106316.
[32] V. Jokinen, P. Suvanto, S. Franssila, Oxygen and nitrogen plasma hydrophilization and hydrophobic recovery of polymers, Biomicrofluidics 6 (1) (2012), 016501, https://doi.org/10.1063/1.3673251.
[33] S. Dou, L. Tao, R. Wang, et al., Plasma-assisted synthesis and surface modification of electrode materials for renewable energy, Adv. Mater. 30 (21) (2018), 1705850, https://doi.org/10.1002/adma.201705850.
[34] J.M. Chen, P.C. Huang, M.G. Lin, Analysis and experiment of capillary valves for microfluidics on a rotating disk, Microfluid. Nanofluid. 4 (2008) 427–437, https://doi.org/10.1007/s10404-007-0196-x.
[35] G. Li, Q. Chen, J. Li, et al., A compact disk-like centrifugal microfluidic system for high-throughput nanoliter-scale protein crystallization screening, Anal. Chem. 82 (11) (2010) 4362–4369, https://doi.org/10.1021/ac902904m.
[36] Q.L. Chen, K.L. Cheung, S.K. Kong, et al., An integrated lab-on-a-disc for automated cell-based allergen screening bioassays, Talanta 97 (2012) 48–54, https://doi.org/10.1016/j.talanta.2012.03.061.
[37] J. Ma, Y. Wu, Y. Liu, et al., Cell-sorting centrifugal microfluidic chip with a flow rectifier, Lab Chip 21 (11) (2021) 2129–2141, https://doi.org/10.1039/D1LC00217A.